Copper-catalyzed, aerobic oxidation of trichloroethyl aryl hydrazonoacetate in a three-phase packed bed reactor

Taylor A. Hatridge[†], Bo Wei[‡], Huw M. L. Davies[‡], Christopher W. Jones[†]*

[‡] Department of Chemistry, Emory University, 1515 Dickey Drive, Atlanta, GA 30322, USA
[†] School of Chemical and Biomolecular Engineering, Georgia Institute of Technology, 311 Ferst Dr., Atlanta, GA 30332-0100, United States

Keywords: continuous processing, diazonium compound, aerobic oxidation, hydrazone, rhodium carbene

Abstract

Copper-catalyzed, aerobic hydrazone oxidation to produce synthetically useful diazonium compounds is achieved in a continuous, three phase flow reactor with complete conversion and high selectivity by adapting a previously published batch methodology to a flow system described herein and conducting a parameter space exploration to optimize the process conditions. The robust nature of the process is demonstrated, with complete hydrazone conversion and a 90% steady-state diazonium compound selectivity maintained over 11 residence times. Employing the diazonium synthesis upstream of a limited scope of dirhodium(II)-catalyzed carbene reactions demonstrates the utility of this process in generating on-demand diazo compounds for cycloaddition and activated secondary C–H insertion reactions. The resulting process represents, to the best of our knowledge, the first reported catalytic process for hydrazone oxidation in flow. Additionally, this process, which only generates water as an oxidative byproduct, is an improvement over previous non-catalytic attempts to synthesize diazo compounds in flow, which generate stoichiometric amounts of waste. The increased sustainability and mitigation of safety hazards associated with handling reactive diazo compounds may make this approach suitable for practical application.

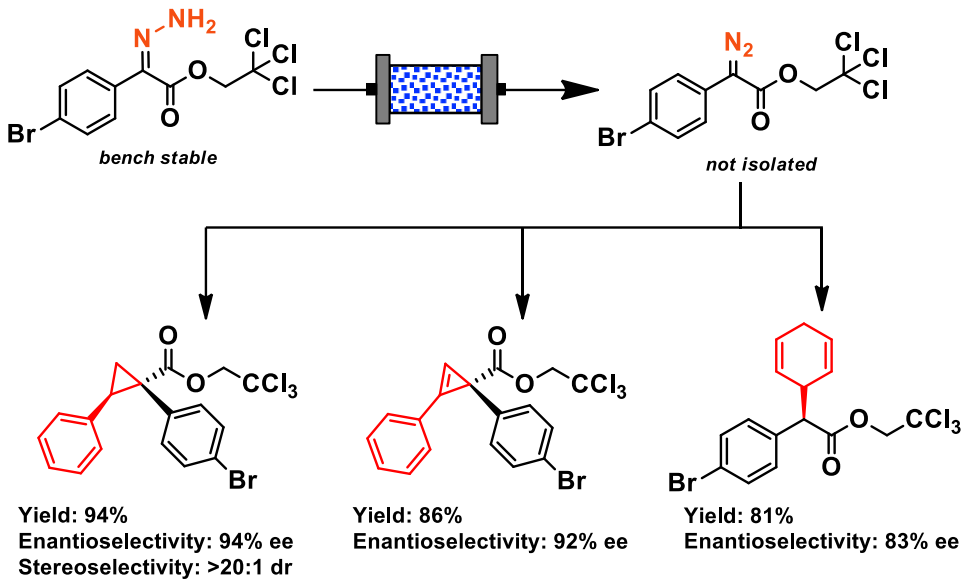

Introduction

In the past two decades, C–H functionalization has created a paradigm shift for organic synthesis by affording new methods to synthesize complex natural products and pharmaceutical molecules.[1-8] In particular, metal carbenes derived from α-diazo carbonyl compounds are synthetically useful, as the thermodynamically favorable evolution of nitrogen gas enables the ready formation of these reactive reagents while forming an environmentally benign byproduct. These donor/acceptor metal carbenes exhibit high reactivity and may undergo a wide range of cycloaddition,[9, 10] X–H insertion (X=O, N, S, Si),[11-13] and C–H insertion reactions with high site- and enantioselectivity,[14] as well as other cross-coupling reactions.[15, 16] Despite the broad synthetic utility of α-diazo carbonyl compounds, their energetic and potentially unstable nature creates safety concerns of exothermic decomposition and possible explosion hazards, limiting the on-site storage and large-scale synthesis of these compounds.[17] As such, only limited examples have demonstrated the use of diazo compounds at large scale.[18-20]

Previous work has sought to address the safety limitation of diazo compounds through flow chemistry. The on-demand synthesis of diazo reagents and their immediate consumption in downstream reactions may obviate safety concerns of on-site storage and/or handling large amounts of diazo compounds in batch reactions. Additionally, flow synthesis may afford access to a greater scope of diazo compounds, including less stable reagents.[21] Previous literature has

achieved diazo synthesis in flow via diazo transfer using tosyl azide,[22, 23] diazotization of primary amines,[24-27] hydrazone fragmentation,[28] and base-catalyzed elimination of diazald.[29-32] However, each of these methodologies generates stoichiometric byproducts and requires large amounts of aqueous base, which may lead to diazo decomposition or undesired reactivity causing interference with downstream reactions, thus requiring in-line separation. In contrast, hydrazone oxidation offers a milder method to generate diazo compounds with water as a benign byproduct, without requiring additional separation steps. These reactions are usually performed using stoichiometric excess of metal oxides, typically MnO_2;[21, 33-36] however, the stoichiometric generation of metal waste, especially for large-scale applications, is undesirable. Hydrazone oxidation has also been conducted in flow using poly(styrene)-supported *N*-iodo-*p*-toluenesulfonamide potassium salt as a stoichiometric oxidant.[37-39] However, iodide leaching interfered with the downstream C–H functionalization[38] and the oxidant must be periodically regenerated with an aqueous KI_3/KOH solution,[37] thus introducing water into the system that could potentially interfere with a downstream C–H insertion. These shortcomings may be absolved with a catalytic process for hydrazone oxidation.

Recently, the Davies and Stahl groups developed a batch methodology using copper(II) acetate hydrate ($Cu(OAc)_2$-H_2O) as a precatalyst under aerobic conditions to oxidize a wide scope of hydrazone compounds to the corresponding aryldiazoacetate in high yields.[40] Building upon this work, we have investigated the application of these reaction conditions to two flow processes: a simple bench-top setup suitable for laboratory applications[41] and a potentially industrially relevant process described herein. In the present study, we seek to develop a continuous process consisting of a three-phase flow system to accommodate the aerobic hydrazone oxidation with immediate consumption of the aryldiazoacetate in a downstream, semi-batch reaction. We investigated the robustness of the process using homogeneous dirhodium (Rh_2L_4) catalysts to conduct some of the classic enantioselective rhodium carbene reactions. To accommodate the Rh_2L_4-catalyzed reactions, some challenges must be accounted for when developing the flow process. First, the Stahl and Davies groups utilized pyridine-derived base additives in tandem with copper to accelerate the reaction rate and improve hydrazone conversion.[40] However, pyridyl groups act as poisons for Rh_2L_4 catalysts due to the strong interaction of the nitrogen atom's lone pair electrons with Lewis acidic metals,[42, 43] which may lead to lower conversion in the downstream reaction.

Additionally, C–H insertion reactions have better performance in solvent sparged with inert gas;[44] this may be an issue as the effluent of our aerobic oxidation stream will be enriched with O_2. The presence of water as a stoichiometric byproduct of the oxidation reaction may introduce some side reactions, notably O–H insertion, in the downstream reaction.[45] Finally, Cu catalysts can react with diazo compounds to form Cu carbenes that may undergo cross-coupling reactions for C–C bond formation.[46] Thus, if appreciable amounts of Cu leach from the column, there could be some catalytic competition that may lower the selectivity of the final product. An awareness of these potential limitations is critical for engineering a robust continuous process for C–H functionalization, and are evaluated in our system design, discussed herein.

Several groups have developed flow systems to accommodate various aerobic oxidation reactions.[47] Previous studies employing homogeneous catalysts for oxidation have found that the reaction rate was limited by the mass transfer of oxygen into the liquid phase, and increasing the surface area of contact between the two phases increased the reaction rate.[48-51] Other studies that employed heterogeneous catalysts in a packed bed with a three-phase reaction found that the hydrodynamic regime has a profound effect on conversion and selectivity.[52-54] Several factors influence the hydrodynamics within a three-phase system, such as the ratio of gas to liquid flow rate, the diameter of particles within the bed, and fluid properties (e.g. surface tension or viscosity).[55] Additionally, the presence of capillary forces increases as reactor diameter decreases, which creates different flow patterns and mass transfer performance in micropacked bed reactors than those observed for industrial scale processes.[52, 56-58]

With these precedents in mind, we developed a milli-scale packed bed reactor design that would enable tuning the flow rates and surface areas of air and liquid phases to study the impact of hydrodynamics on the aerobic oxidation. We found that operating in a gas-continuous regime was important for maximizing oxidation and system performance was maintained over 11 residence times. The utility of this system is demonstrated by placing the hydrazone oxidation upstream of the various carbene reactions. To the best of our knowledge, this report is the first to describe a catalytic, aerobic oxidation of hydrazone compounds in flow.

Results and Discussion

To adapt the Cu-catalyzed aerobic oxidation of hydrazone compounds to a flow system, we focused on the oxidation of 2,2,2-trichloroethyl (*Z*)-2-(4-bromophenyl)-2-hydrazonoacetate **1** to 2,2,2-trichloroethyl 2-(4-bromophenyl)-2-diazoacetate **2** (**Figure 1**). This was chosen as a model substrate because the diazo compound **2** has been demonstrated to be a robust reactant in various C–H insertion reactions, exhibiting excellent reactivities and selectivities.[59] We utilized 4-(*N,N*-dimethylamino)pyridine (DMAP) as a basic additive because its increased basicity and nucelophilicity over pyridine offers a faster reaction rate,[40] which could lower the residence time required to achieve maximum conversion in a flow system. Dichloromethane (DCM) was used as the reaction solvent and silica was used as an additive in the packed bed, along with the $Cu(OAc)_2$-H_2O precatalyst.

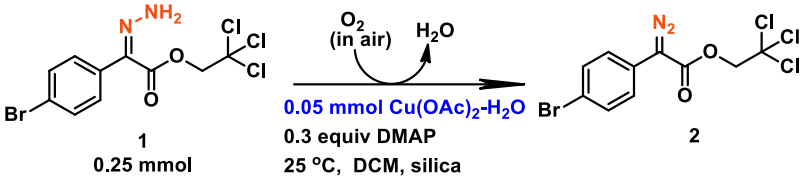

Figure 1. Reaction conditions for aerobic oxidation of 2,2,2-trichloroethyl (*Z*)-2-(4-bromophenyl)-2-hydrazonoacetate in flow

Before implementing the hydrazone oxidation reaction in flow, the $Cu(OAc)_2$-H_2O precatalyst was probed in batch conditions to give insight into the homogeneous or heterogeneous nature of the catalyst via a split test (**Figure 2**). To conduct the split test, two reactions were set up using the same conditions; however, one reaction was filtered through a short silica plug after 3 minutes, whereas the other was left undisturbed. Upon filtration of the reaction media, reaction progress was arrested, as the Cu was visibly retained in the silica plug and hydrazone conversion remained at 66%. In contrast, the unfiltered sample reached complete conversion of hydrazone in less than ten minutes.

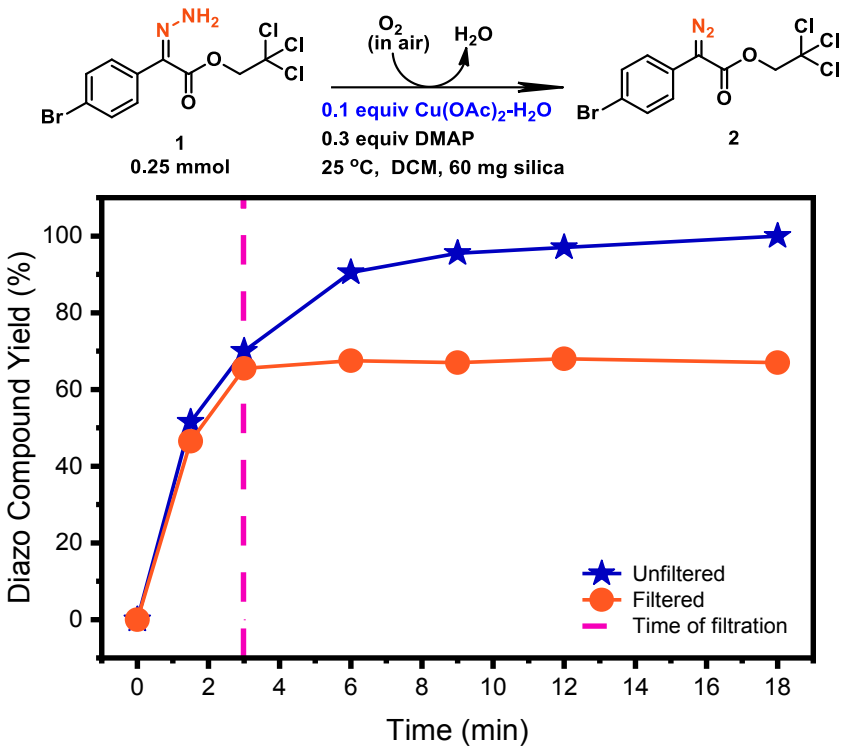

Figure 2. Split test results for batch hydrazone oxidation. The dashed line indicates time of filtration (3 minutes) through a short silica plug for the filtered sample. Diazo compound yield was calculated via quantitative NMR using dodecane as an internal standard.

According to the previous batch study, the $Cu(OAc)_2$-H_2O precatalyst exhibited low solubility in DCM, necessitating the inclusion of organic bases to solubilize the Cu catalyst.[40] Thus, the retention of Cu in the silica plug may be due to low solubility in DCM or polar interaction with the silanol surface. Previous literature has shown that Cu(II) salts sorb to polar support materials in various solvents with low leaching.[60-62] Additionally, a computational study by Musaev and Liebeskind demonstrated that Cu carboxylates coordinate strongly with thiolate sulfur atoms, and this coordination is energetically favorable.[63] Thus, it is possible that a silica-sorbed Cu structure acts as a precatalyst, and DMAP-solubilized Cu is the active catalyst.

The reversible sorption of the Cu catalyst to the silica surface would combine the effects of homogeneous and heterogeneous catalysts, namely fast reaction times and facile catalyst isolation, and support the feasibility of its implementation in a flow condition using a silica packed bed. Previous studies have implemented "catch and release" catalysts in flow reactors using strategies such as reverse-flow adsorption or release/capture columns in series.[64] In our reaction setup

(explained in more detail in **Figure 3**), the $Cu(OAc)_2$-H_2O precatalyst is mixed with an excess of silica and placed over a silica plug, which acts as a reservoir to capture the solubilized Cu catalyst from the reaction stream. This study does not utilize two separate capture/release columns with a reversible flow path; however, future studies investigating the implementation of this chemistry in a larger scale process may find this type of setup useful.

The flow setup for our process accommodates three-phases in a glass column, as shown in **Figure 3**. The milliscale reactor has a radius of 5 mm and bed length of 5 cm. A syringe pump containing hydrazone and DMAP dissolved in DCM pushes the liquid phase into the top of the glass column. The oxygen is supplied via an ultra-zero air cylinder, which is within the safe flammability limits for DCM[47] and avoids introduction of additional water into the system, which could introduce O–H insertion side reactions. The flow rate of air into the column is controlled by a gas flow control meter. The headspace of the column is packed with glass wool to facilitate mixing between the co-current gas and liquid streams before the fluid phase enters the solid $Cu(OAc)_2$-H_2O/silica packed bed. The catalyst bed contains 0.05 mmol of $Cu(OAc)_2$-H_2O mixed with 60 mg of silica atop 500 mg of silica, which is supported by a glass frit. To optimize the flow procedure, we utilized "pulse" experiments as a quick diagnostic tool to evaluate process performance at various conditions. For each pulse, 0.25 mmol of hydrazone at a specific concentration was introduced into a sampling loop of tubing, which was then pushed through the column using DCM in the syringe pump. More details about the pulse experiments are described in the Experimental Section.

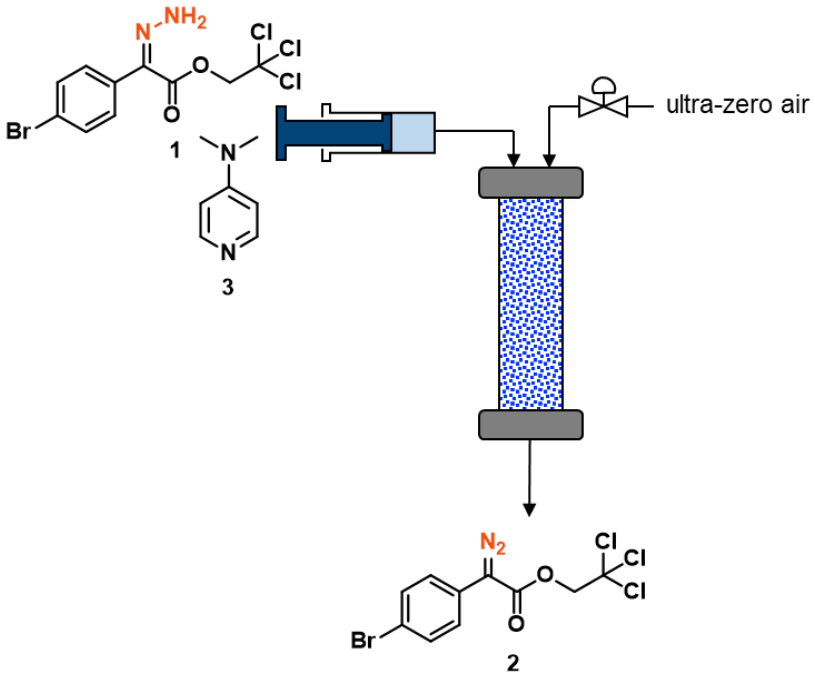

Figure 3. Flow setup for continuous processing of diazo compounds. The hydrazone and DMAP solution are introduced to the top of the column via a syringe pump, while the ultra-zero air flow rate is controlled using a mass flow controller. The co-current downflow of air and liquid enters into the packed bed of $Cu(OAc)_2$-H_2O precatalyst and silica, and the resulting diazo compound elutes from the column.

In determining a flow procedure, we first examined the role of DMAP **3** in the reaction stream. Because DMAP poisons Rh_2L_4 catalysts,[42, 43] we wanted to investigate the possibility of maximizing aryldiazoacetate yield while minimizing DMAP concentration in the reaction stream. We found that rinsing the column with 0.5 mL of a 0.3 M DMAP solution before introducing the hydrazone/DMAP stream increased the yield of diazo compound, while allowing a reduction in the amount of DMAP included in the reaction stream (**Table 1**). In all cases with the DMAP pre-rinse, the yield of aryldiazoacetate was higher (29-56%) than with a pre-rinse consisting only of solvent (19%). However, the inclusion of DMAP in stoichiometric excess of Cu in the reaction stream was necessary to regenerate the active catalyst and maintain aryldiazoacetate yield. Decreasing the amount of DMAP in the inlet stream from 0.6 to 0.3 equivalents to hydrazone did not show a reduction in yield, but further decreasing DMAP from 0.3 to 0.1 equivalents resulted in a significant decrease in yield, from 55% to 29%. Therefore, moving forward with optimizing the flow process conditions, we employed a prewash of 0.5 mL of 0.3 M solution of DMAP in DCM and included 0.3 equivalents of DMAP with the hydrazone stream to maintain a high

aryldiazoacetate yield while minimizing the possible poison for downstream Rh_2L_4-catalyzed reactions.

Table 1. Effect of DMAP on reaction performance (L=1 mL/min, G=17.5 mL/min, C=0.5 M)

Entry	Pre-wash	DMAP Equivalents in Pulse[a]	Diazo Compound Yield[b] (%)
1	DCM only	0.6	19
2	0.3 M DMAP solution	0.6	56
3	0.3 M DMAP solution	0.3	55
4	0.3 M DMAP solution	0.1	29

[a] Equivalents in reference to the 0.25 mmol of hydrazone in the pulse. [b] Diazo compound yield was calculated via quantitative nuclear magnetic resonance (NMR) spectroscopy using dodecane as an internal standard.

Next in optimizing flow conditions, we chose to evaluate the importance of three variables in influencing aryldiazoacetate yield: air and liquid flow rates and hydrazone concentration. High and low values of each variable were chosen, as shown in **Table 2**, to explore a parameter space and determine the relative effect of each variable on the process performance. Simultaneously varying these parameters in a body-centered design allowed us to efficiently investigate how each variable influenced the others, along with aryldiazoacetate yield. Several studies have utilized this approach to successfully optimize flow processes, especially for industrial and pharmaceutical applications.[65-68]

In our case, specific boundary values for each variable were determined based on practical limitations of the design space. The minimum air flow rate (G) was chosen as 7 mL/min based on the lower range of the gas flow control meter; the maximum air flow rate was chosen as 17.5 mL/min because a higher G would have dried the packed bed, resulting in incomplete catalyst utilization due to reduced catalyst wetting.[69] The boundary values for the liquid flow rate (L) were chosen so as to traverse different hydrodynamics regimes based on the given air flow rates. The minimum hydrazone concentration (C) value was chosen to be 0.25 M because the tubing going into the reactor could accommodate a maximum volume of 1 mL of sample; the high concentration value was chosen as 0.5 M because increasing the hydrazone concentration past that point led to limited solubility. Additionally, the midpoint of the parameter space (G = 12.25 mL/min, L = 0.625 mL/min, C = 0.375 M) was performed three times to ensure the repeatability of the flow process.

The midpoint results showed an aryldiazoacetate yield of 69 ± 3%. The low standard deviation indicates that the process is repeatable.

Table 2. Values for variables of interest in parameter space exploration

Process Variable	High/Low	Boundary value
Air Flow Rate (mL/min)	High	17.5
	Low	7
Liquid Flow Rate (mL/min)	High	1
	Low	0.25
Hydrazone Concentration (M)	High	0.5
	Low	0.25

The results of the parameter space exploration are shown graphically in **Figure 4**. (A table of the full results is included in the SI.) **Figure 4A** shows the effect of liquid flow rate on aryldiazoacetate yield; **Figure 4B** shows the effect of air flow rate; and **Figure 4C** shows the effect of hydrazone concentration. In each graph, each data series corresponds to a consistent set of flow conditions in regard to the other two variables.

According to these results, liquid flow rate is the most influential variable, as decreasing liquid flow rate from 1 mL/min to 0.25 mL/min resulted in a substantial increase in aryldiazoacetate yield in each instance (**Figure 4A**). This observed increase is likely because decreasing liquid flow rate increases the residence time of hydrazone in the catalyst packed bed, allowing more time for the oxidation reaction to occur. The most dramatic increases in yield were observed at the lower gas flow rate (G = 7 mL/min). At these flow rates, the yield for C = 0.25 M condition increased from 31% at L = 1 mL/min to 81% at 0.25 mL/min; for the C = 0.5 M condition, the yield increased from 48% at 1 mL/min to 87% at 0.25 mL/min. This observation is likely because lowering the liquid flow rate at the low air flow rate also improved external mass transfer of O_2 into the liquid phase in addition to increasing the residence time.

Increasing the air flow rate from 7 mL/min to 17.5 mL/min had a negligible to moderate effect on aryldiazoacetate yield at low liquid flow rates (**Figure 4B**). However, the effect of air flow rate became more pronounced at high liquid flow rates, again likely due to increased external mass transfer of O_2 into the liquid phase. The most significant effect corresponds to conditions of L = 1 mL/min and C = 0.25 M, where diazo compound yield increased from 31% at an air flow rate of 7 mL/min to 57% at 17.5 mL/min. The interplay of air and liquid flow rates was explored by investigating the ratio of gas to liquid flow rate (G:L) on diazo compound yield, which is pictured in **Figure 4D** and discussed in more detail below.

Finally, varying the hydrazone concentration (**Figure 4C**) exhibits a negligible effect on aryldiazoacetate yield, with the exception of the conditions at G = 7 mL/min and L = 1 mL/min. At these flow rates, diazo compound yield increases from 31% at C = 0.25 M to 48% at C = 0.5 M. The increased influence of concentration at these flow conditions is possibly because the short residence time (due to the high liquid flow rate) and low O_2 mass transfer (due to the low air flow rate) result in kinetic limitations that are partially alleviated by doubling the concentration.

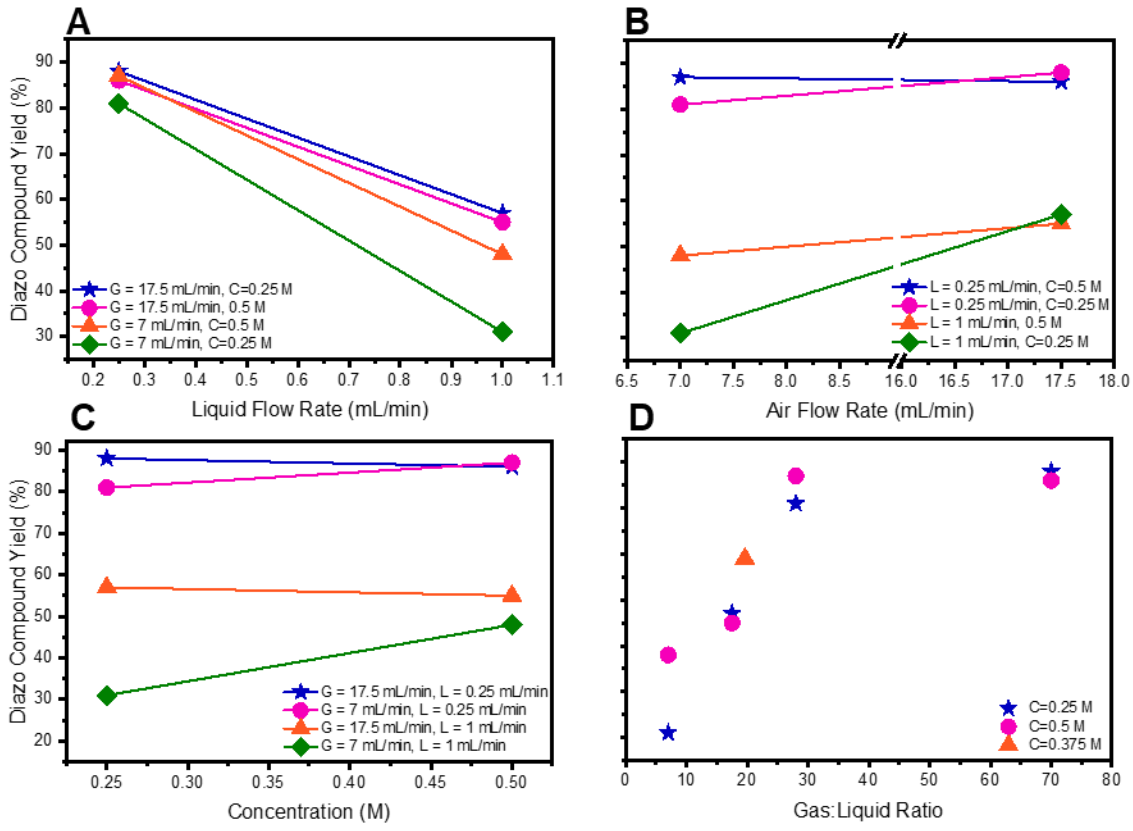

Figure 4. Results from the parameter space exploration showing the effects of air and liquid flow rate, hydrazone concentration, and gas to liquid flow rate (G:L) ratio on aryldiazoacetate yield. Each data series represents a consistent set of two variables to examine the influence of changing one variable (presented on the x-axis) on aryldiazoacetate yield. Diazo compound yield was calculated via quantitative NMR using dodecane as an internal standard. (A) Effect of liquid flow rate. (B) Effect of air flow rate. (C) Effect of concentration. (D) Effect of the ratio of gas to liquid flow rate (G:L), or hydrodynamics, on aryldiazoacetate yield.

Figure 4D shows the ratio of gas to liquid flow rate (G:L) and the effect of this ratio on aryldiazoacetate yield, showing that increasing G:L results in an increase in yield at lower ratios (at or below 19.6), which plateaus at 88% for higher ratios (at or above 28). Qualifying the hydrodynamic regime within the packed bed at each of these points helps to explain this trend. Studies on micropacked bed reactors have shown that different hydrodynamic regimes exist at small scale compared to industrial scale packed bed reactors.[56, 58] Thus, due to the small scale of our reactor, we looked to the flow regime maps published by Gavriilidis *et. al.* to determine the hydrodynamics within our system. Although our reactor is slightly larger in scale than that utilized by Gavriilidis in their study, the low Re (0.0034-0.034), Bo (1.19×10^{-4}), and Ca (3.22×10^{-8} to 3.22×10^{-7}) numbers corresponding to our conditions are of a similar magnitude as the Gavriilidis system.[52] Additionally, these low values show the prevalence of capillary forces and laminar flow in our system, making a comparison to the hydrodynamics of microscale more appropriate than to industrial scale.

Table 3 lists the hydrodynamics regimes of each G:L ratio listed in **Figure 4D**. At a G:L of 7, the liquid stream dominates the continuous phase with some gas slugs interspersed;[52] therefore, the low interfacial area between the gas and liquid phases at these flow conditions corresponds to the low oxidative yield. At G:L of 17 and 19.6, a segregated flow regime is present, whereby gas and liquid phases share a relatively even volume of the packed bed, corresponding to a thick liquid film with more gas phase interspersed.[52] This results in a higher surface area of contact between the gas and liquid phases, offering greater mass transfer of oxygen into the reaction phase, resulting in higher yield of diazo compound in this regime. A G:L of 28 is at the transition point from segregated to gas-continuous flow. Above this point (at G:L = 70), there is no further increase in aryldiazoacetate yield. The gas-continuous flow regime consists of a continuous gas phase with a thin liquid film distributed over the solid particles in the packed bed.[52] The decrease in liquid film

thickness results in a higher interfacial area between the liquid and air phases, affording a further increase in mass transfer of oxygen into the liquid phase and resulting in the highest oxidative yield observed at these conditions of 88%.

Table 3. Hydrodynamic regimes encountered at different air and liquid flow rates.

Entry	Air Flow Rate (mL/min)	Liquid Flow Rate (mL/min)	G:L	Predicted Flow Regime[52]	Analogous to (in macroscale)
1	7	1	7	Liquid-dominated slug	Pulse
2	17.5	1	17.5	Segregated	Trickle (thick liquid film)
3	12.25	0.625	19.6	Segregated	Trickle (thick liquid film)
4	7	0.25	28	Segregated to gas-continuous flow transition	Trickle (intermediate liquid film)
5	17.5	0.25	70	Gas-continuous (fully wetted)	Trickle (thin film / rivulet)
6	7	0.1	70	Gas-continuous (fully wetted)	Trickle (thin film / rivulet)

We then used the results from the parameter exploration to determine our optimized flow conditions. The optimized flow rates were achieved by lowering the liquid flow rate to increase the residence time, while maintaining a high G:L so as to remain in the gas-continuous flow regime. A liquid flow rate of 0.1 mL/min and air flow rate of 7 mL/min achieved these requirements. Another pulse study using these conditions and a hydrazone concentration of 0.5 M confirmed nearly complete conversion of hydrazone compound (99%) with a 93% yield of diazo compound. Repeating this experiment using the same flow rates and a concentration of 0.25 M gave a similar result (99% conversion and 94% yield). These results correspond well with the literature result from the previous Stahl and Davies work in batch.[40]

Figure 5 shows a residence time distribution (RTD) at these optimized air and liquid flow rates, which was generated using a step impulse of 0.25 M aryldiazoacetate solution at time $t = 0$. The residence time, τ, was calculated to be 7.85 min based on the catalyst bed dimensions and flow rate of the liquid stream. The following equations[70] were used to fit an nCSTR model to the step impulse timepoints:

$$\Theta = {}^{t}/_{\tau} \quad (1)$$

$$E(\theta) = \frac{C_n}{C_o} = \frac{n^n \theta^{n-1}}{(n-1)!} e^{-n\theta} \quad (2)$$

$$F(\theta) = \int_0^\theta E(\theta)\, dt \quad (3)$$

To fit the nCSTR model to the step impulse data, the sum of squared error of **Equation 3** was minimized relative to the data by iterating through separate values of n (number of CSTRs). According to this fit, the flow eluting from our column is simulated as six CSTRs in series. An n below twenty CSTRs indicates deviation from ideal plug flow behavior. In this case, nonideal behavior is likely caused by channeling in the packed bed, which is common in three-phase operations.[55] Additionally, the generated F curve did not align with the plotted step impulse data, likely due to adsorption of the diazo compound to the silica in the packed bed, which delays the elution of aryldiazoacetate from the column. Shifting the fit curve by 0.3 residence times generates an excellent fit, as shown in **Figure 5**. Insight into the adsorption behavior can be gleaned from the time delay of 0.3 residence times. Within this time frame, according to the given solution concentration and flow rate, 0.06 mmol of aryldiazoacetate would be sorbed to the 560 mg of silica (surface area of 500 m^2/g) present in the column, yielding sorption behavior of 0.1 $mmol_{diazo}/g_{silica}$, or 2.1×10^{-4} $mmol_{diazo}/m^2_{silica}$.

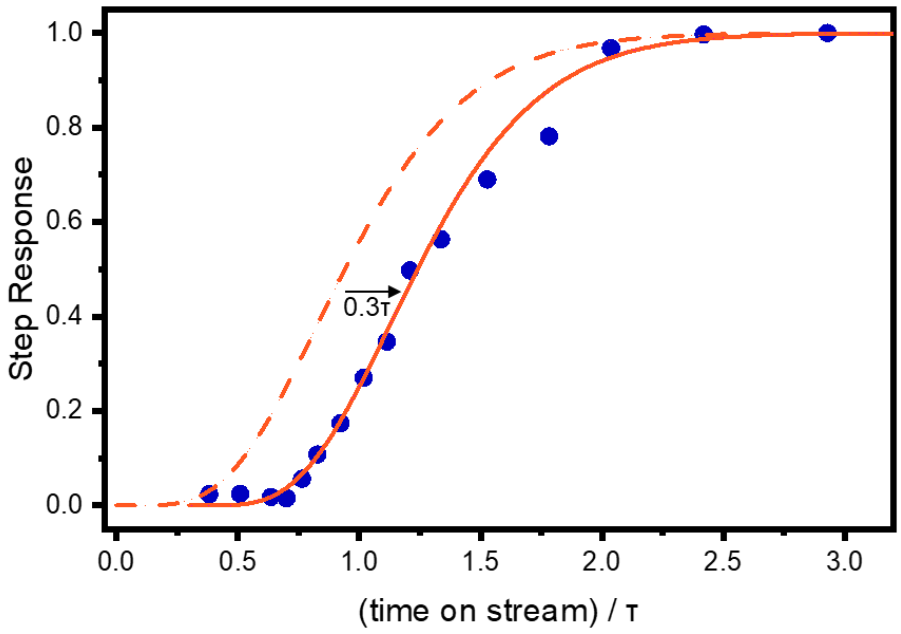

Figure 5. Residence time distribution curve showing response associated with the step change from a DCM solution to a 0.25 M aryldiazoacetate solution at time t = 0 through the packed bed

at L = 0.1 mL/min and G = 7 mL/min. The reactor effluent was collected in timepoints and the concentration of diazo compound in the effluent was monitored via *ex situ* UV-Vis spectroscopy. The absorbance peak was normalized to the maximum aryldiazoacetate concentration of the step response (0.25 M). Fitting to an nCSTR model gives n = 6. Shifting the fit curve to the right by 0.3 residence times captures the phenomenon of adsorption of diazo compound to the silica in the packed bed.

With the optimized conditions in hand, we next explored the performance of the process during a continuous flow procedure over a longer time scale. **Figure 6A** shows the conversion of hydrazone starting material and selectivity for aryldiazoacetate product over 10.8 residence times using the following conditions: G = 7 mL/min, L = 0.1 mL/min, and C = 0.25 M. These results show that the complete conversion of hydrazone was maintained over the entire time on stream. However, as the time on stream progressed, the selectivity for aryldiazoacetate product decreased gradually from 100% to a steady state selectivity of 90% after 4.5 residence times. NMR analysis showed that some byproduct formation was due to an O–H insertion reaction between water and the aryldiazoacetate product (likely due to the build-up of water as an oxidation byproduct as the reaction progressed), as well as some dimerization of the diazo compound. Based on these results, the TON was determined to be 74.

Figure 6B shows the elution of each compound from the reactor over time. Aryldiazoacetate concentration reaches its steady state value of 0.23 M at 3.2 residence times. DMAP begins to elute from the column after 8.3 residence times with a final concentration of 0.29 M at 10.8 residence times. This concentration is higher than that of the DMAP in the reaction solution (0.075 M). Therefore, the delayed elution is likely due to polar interactions between DMAP and the silica surface, which slow the travel of DMAP through the packed bed in an effect similar to column chromatography. The retention of DMAP within the silica bed supports the validity of employing the freshly synthesized diazo compound in a downstream rhodium-carbene reaction without poisoning the Rh_2L_4 catalyst for a time on stream of less than 8.3 residence times. Some Cu leaching (about 5 ppm) was observed throughout most of the reaction progress; however, the Cu largely does not elute from the column until longer time scales, with the timepoints at 9.5 residence times containing 25 ppm of Cu and 10.8 residence times containing 82 ppm of Cu. Again, this delayed elution is likely due to the interaction of the Cu catalyst with the polar silica surface. The

strong interaction between the Cu and silica for extended times also further corroborates our earlier observations seen during the split test shown in **Figure 2**.

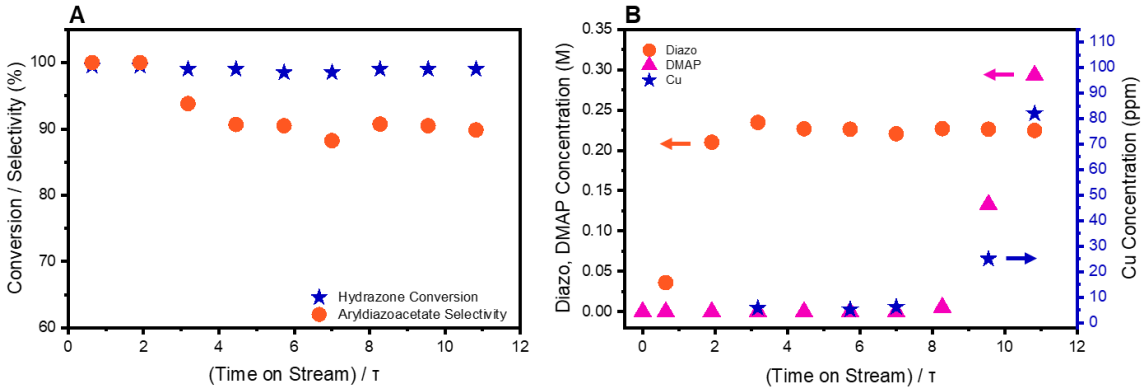

Figure 6. Performance of hydrazone oxidation process over 10.8 residence times. (A) Complete hydrazone conversion is maintained throughout time on stream and steady state aryldiazoacetate selectivity reaches 90% at 4.5 residence times. Hydrazone conversion and aryldiazoacetate selectivity were calculated via quantitative NMR using dodecane as an internal standard. (B) Elution of reaction components from the reactor. Aryldiazoacetate concentration in the effluent was calculated via quantitative NMR using dodecane as an internal standard and was confirmed by integrating the RTD shown in Figure 5; DMAP concentration was calculated via quantitative NMR using dodecane as an internal standard; Cu concentration was quantified using ICP-OES elemental analysis.

Building upon our continuous process, we included a semi-batch, dirhodium-carbene reaction for immediate consumption of the diazo compound downstream of the flow reaction. The semi-batch setup and Rh_2L_4 catalyst structures we employed are shown in **Figure 7A**. To conduct the semi-batch reactions, a round bottom flask was equipped with the appropriate substrate and 1 mol% of the Rh_2L_4 catalyst, along with activated 4Å molecular sieves to capture water that may interfere with the carbene reaction, and connected to the flow reactor effluent.

We performed several different dirhodium-carbene reactions to probe the robustness of this continuous process, as shown in **Figure 7B**. A cyclopropanation reaction with styrene gave a very high yield of 94% and enantioselectivity of 94% ee. This result is an improvement over the 67% yield observed in the tandem batch reaction employed in the previous Davies, Stahl work,[40] which demonstrates the utility of this continuous process over batch reactions in series. Similarly, a

cyclopropenation with ethynylbenzene[71] gave a good yield of 86% and high enantioselectivity of 92% ee.

Cyclohexa-1,4-diene was used as an activated substrate for secondary C–H insertion.[72] Moderate yield (64%) and enantioselectivity (71% ee) were observed. Previous studies have shown that addition of 1,1,1,3,3,3-hexafluoro-2-propanol (HFIP) improved reaction performance in rhodium carbene-catalyzed reactions.[73-75] The addition of 20 equivalents of HFIP to the semi-batch reaction mixture resulted in an increased C–H insertion yield of 81% and higher selectivity of 83% ee. Finally, we explored the performance of secondary C–H insertion using an unactivated substrate, in this case cyclohexane. At room temperature, the reaction had excellent enantioselectivity of 99% ee, albeit with a low yield of 32% due to carbene dimer formation as a significant byproduct. The addition of HFIP did not improve reaction performance for this substrate, due to the already observed high enantioselectivity. Increasing the temperature of the reaction to 50 °C increased the yield slightly to 51%; however, the higher temperature was detrimental to the enantioselectivity, which decreased dramatically to 52% ee. The dirhodium-catalyzed C–H insertion of unactivated substrates is highly sensitive to the reaction condition. For this system, the presence of water and trace DMAP in the solution necessitates further optimization to promote the C–H insertion, and further substrates were not employed in this initial work.

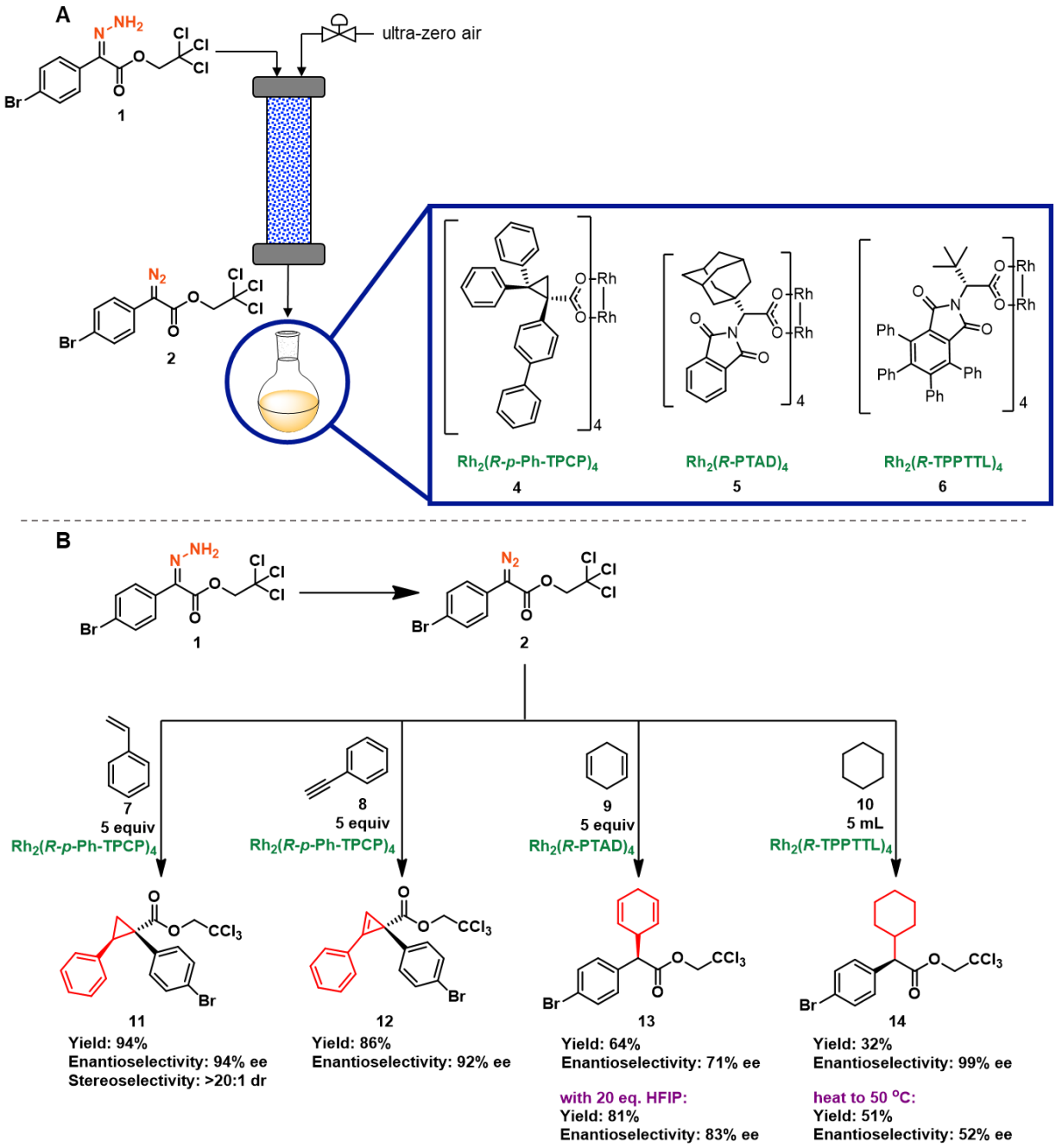

Figure 7. (A) Semi-batch set-up showing the connection of the flow reactor effluent to a round bottom flask containing the appropriate substrate, Rh_2L_4 catalyst, and activated 4 Å molecular sieves. The Rh_2L_4 catalyst structures employed in the C–H insertion reactions are shown. (B) Results of the semi-batch reaction scope. Each reaction was performed at room temperature using 1 mol% of Rh_2L_4 catalyst and 5 equivalents of substrate, unless otherwise noted. The isolated yield is calculated relative to the 0.25 mmol of hydrazone fed into the flow reactor.

Conclusion

In this study, we developed a catalytic flow process for the aerobic oxidation of hydrazone to diazo compounds. Our three-phase reactor utilizes co-current downflow of air and liquid streams through a packed bed of silica and $Cu(OAc)_2$-H_2O precatalyst. The performance of the flow system was strongly dependent on air and liquid flow rates, which influenced the hydrodynamics within the packed bed, with a high ratio of air to liquid flow rate important for maximizing aryldiazoacetate yield. A time on stream experiment showed that DMAP and Cu did not begin to elute from the column until 9 residence times. Successful process performance was maintained over 11 residence times, with complete hydrazone conversion for the entire time on stream and a steady-state aryldiazoacetate selectivity of 90%. Finally, we employed our flow process upstream of several semi-batch, dirhodium-catalyzed reactions for immediate consumption of the freshly synthesized diazo compound. This continuous process was compatible with multiple dirhodium catalysts and showed high yield and enantioselectivity for cyclopropanation, cyclopropenation, and activated secondary C–H insertion reactions.

To the best of our knowledge, the process described herein is the first example of a catalytic, aerobic oxidation of hydrazone compounds to achieve diazo compound synthesis in flow. The successful implementation of this system absolves some shortcomings of other previously published methods to synthesize diazo compounds in flow, which typically generate stoichiometric byproducts or require strong bases or stoichiometric quantities of metal oxides. In contrast, our system utilizes oxygen (from air) as a sustainable oxidant and generates water as a green byproduct. Additionally, the use of catalytic amounts of copper and high selectivity for the aryldiazoacetate product makes this an atom-efficient process that generates low amounts of waste. This, as well as the demonstrated utility of this process to synthesize diazo compounds as precursors for C–H functionalization reactions, may alleviate some of the concerns that have hindered industrial adoption of C–H functionalization as a synthetic method due in part to safety concerns associated with handling reactive diazo compounds.

Experimental Details

Materials, analytical tools and instrumentation, split test procedures, column dimensions and packing procedure, residence time distribution procedure and analysis, product characterization,

and HPLC procedures are detailed in the Supporting Information. General procedures for the reactions conducted in flow are detailed below.

Pulse reaction. To conduct each pulse reaction, the syringe pump upstream of the reactor was fitted with a 10 mL syringe containing 8 mL of degassed, anhydrous DCM. The packed bed was first rinsed with 1 mL of DCM provided via the syringe pump at the specified liquid flow rate. Then, 0.5 mL of 0.3 M DMAP in DCM was then injected into the PTFE tubing and pushed through the packed bed by an additional 0.5 mL of DCM. Finally, a pulse of 0.25 mmol of hydrazone, 0.075 mmol of DMAP (0.3 equiv.), and 50 μL of dodecane were dissolved in DCM at the specified concentration (0.5 mL for 0.5 M or 1 mL for 0.25 M) and injected into the PTFE tubing. The flow reaction was then conducted at the specified air and liquid flow rates. The column was rinsed with 5 mL of DCM to ensure complete recovery of the hydrazone/diazo solution from the column into a glass vial for collection. The extent of reaction was determined via ^{1}H-NMR in $CDCl_3$ using dodecane as an internal standard.

Time on Stream. The procedure for the time on stream experiment is similar to that of the pulse reaction. The column is setup and rinsed with degassed, anhydrous DCM and a 0.3 M DMAP solution as described previously. After the pre-rinse, a 10 mL syringe containing 2 mmol of hydrazone, 0.6 mmol of DMAP (0.3 equiv.), and 400 μL of dodecane dissolved in 8 mL of DCM was placed in the syringe pump. The reaction was carried out using a liquid flow rate of 0.1 mL/min and air flow rate of 7 mL/min. Timepoints were taken by switching the reactor's exit tubing to a new vial every ten minutes. Hydrazone conversion, diazo yield, and the concentration of diazo and DMAP eluting from the column were calculated via ^{1}H-NMR in $CDCl_3$ using dodecane as an internal standard. The elution concentration of the diazo compound was confirmed via integration of the previously generated RTD curve. The concentration of Cu in the reactor effluent was determined using ICP-OES analysis conducted by Galbraith Laboratories. These data are reported as an average value over the ten-minute timepoint.

General Semi-batch Procedure. To conduct each semi-batch reaction, a 50 mL round bottom flask was equipped with a magnetic stir bar and flame dried. Activated 4 Å molecular sieves (4 g; dried at 200 °C and 10 mTorr overnight) were added to the flask, which was fitted with a septum and

back filled with N_2. Additional care was taken to prevent introduction of water into this reaction by further drying anhydrous, degassed DCM on activated 4 Å molecular sieves overnight. (For the cyclohexane reaction, the 5 mL of cyclohexane employed as the substrate was also degassed and dried on activated 4 Å molecular sieves overnight.) The appropriate dirhodium catalyst and substrate were each dissolved in 1 mL of this dry, degassed DCM and injected into the round-bottom flask, along with an additional 3 mL of DCM. This reaction mixture was stirred for ten minutes to ensure a homogeneous solution. The flow reaction was set up using the previously described pulse procedure, with the reactor effluent connected to the septum of the round bottom flask. The semi-batch reaction solution was sparged with N_2 during reaction to minimize deleterious effects of dissolved O_2 in the reactor effluent on dirhodium catalyst performance. Upon completion of the pulse diazo synthesis, the semibatch inlet and N_2 sparge were removed and the semibatch reaction proceeded overnight under inert atmosphere. The resulting reaction products were isolated and characterized via HPLC as described in the Supplementary Information.

Acknowledgements

Financial support was provided by NSF under the CCI Center for Selective C–H Functionalization (CHE-1700982) and by an additional NSF grant (CHE-1956154) the NSF Graduate Research Fellowship Program (DGE-1650044).

References

1. Godula, K.; Sames, D., C–H Bond Functionalization in Complex Organic Synthesis. *Science* **2006,** *312* (5770), 67-72.
2. Colby, D. A.; Bergman, R. G.; Ellman, J. A., Rhodium-Catalyzed C-C Bond Formation via Heteroatom-Directed C-H Bond Activation. *Chem. Rev.* **2010,** *110*, 624–655.
3. Colby, D. A.; Tsai, A. S.; Bergman, R. G.; Ellman, J. A., Rhodium Catalyzed Chelation-Assisted C—H Bond Functionalization Reactions. *Acc. Chem. Res.* **2011,** *45* (6), 814–825.
4. Gutekunst, W. R.; Baran, P. S., C-H functionalization logic in total synthesis. *Chem. Soc. Rev.* **2011,** *40* (4), 1976-1991.
5. Yamaguchi, J.; Yamaguchi, A. D.; Itami, K., C-H bond functionalization: emerging synthetic tools for natural products and pharmaceuticals. *Angew. Chem. Int. Ed.* **2012,** *51* (36), 8960-9009.
6. Wencel-Delord, J.; Glorius, F., C-H bond activation enables the rapid construction and late-stage diversification of functional molecules. *Nat. Chem.* **2013,** *5*, 369-75.
7. Noisier, A. F.; Brimble, M. A., C-H functionalization in the synthesis of amino acids and peptides. *Chem. Rev.* **2014,** *114* (18), 8775-8806.
8. Davies, H. M.; Morton, D., Recent Advances in C-H Functionalization. *J. Org. Chem.* **2016,** *81* (2), 343-350.
9. Zhang, B.; Davies, H. M. L., Rhodium-Catalyzed Enantioselective [4+2] Cycloadditions of Vinylcarbenes with Dienes. *Angew. Chem.* **2020,** *132*, 4967-4971.

10. Negretti, S.; Cohen, C. M.; Chang, J. J.; Guptill, D. M.; Davies, H. M. L., Enantioselective Dirhodium(II)-Catalyzed Cyclopropanations with Trimethylsilylethyl and Trichloroethyl Aryldiazoacetates. *Tetrahedron* **2015,** *71*, 7415-7420.
11. Gillingham, D.; Fei, N., Catalytic X-H insertion reactions based on carbenoids. *Chem. Soc. Rev.* **2013,** *42* (12), 4918-4931.
12. Harada, S.; Tanikawa, K.; Homma, H.; Sakai, C.; Ito, T.; Nemoto, T., Silver-Catalyzed Asymmetric Insertion into Phenolic O-H Bonds using Aryl Diazoacetates and Theoretical Mechanistic Studies. *Chem. Eur. J.* **2019,** *25*, 12058-12062.
13. Tanbouza, N.; Keipour, H.; Ollevier, T., FeII-catalysed insertion reaction of α-diazocarbonyls into X–H bonds (X = Si, S, N, and O) in dimethyl carbonate as a suitable solvent alternative. *RSC Adv.* **2019,** *9*, 31241-31246.
14. Davies, H. M.; Liao, K., Dirhodium tetracarboxylates as catalysts for selective intermolecular C–H functionalization. *Nat. Rev. Chem.* **2019,** *3*, 347−360.
15. Wang, D.; Szabo, K. J., Copper-Catalyzed, Stereoselective Cross-Coupling of Cyclic Allyl Boronic Acids with alpha-Diazoketones. *Org. Lett.* **2017,** *19* (7), 1622-1625.
16. Xia, Y.; Qiu, D.; Wang, J., Transition-Metal-Catalyzed Cross-Couplings through Carbene Migratory Insertion. *Chem. Rev.* **2017,** *117* (23), 13810-13889.
17. Green, S. P.; Wheelhouse, K. M.; Payne, A. D.; Hallett, J. P.; Miller, P. W.; Bull, J. A., Thermal Stability and Explosive Hazard Assessment of Diazo Compounds and Diazo Transfer Reagents. *Org. Process Res. Dev.* **2020,** *24*, 67-84.
18. Anthes, R.; Bello, O.; Benoit, S.; Chen, C.; Corbett, E.; Corbett, R. M.; DelMonte, A. J.; Gingras, S.; Livingston, R.; Sausker, J.; Soumeillant, M., Kilogram Synthesis of a Selective Serotonin Reuptake Inhibitor. *Org. Process Res. Dev.* **2008,** *12* (2), 168-177.
19. Gage, J. R.; Chen, F.; Dong, C.; Gonzalez, M. A.; Jiang, Y.; Luo, Y.; McLaws, M. D.; Tao, J., Semicontinuous Process for GMP Manufacture of a Carbapenem Intermediate via Carbene Insertion Using an Immobilized Rhodium Catalyst. *Org. Process Res. Dev.* **2020,** *24* (10), 2025-2033.
20. Bien, J.; Davulcu, A.; DelMonte, A. J.; Fraunhoffer, K. J.; Gao, Z.; Hang, C.; Hsiao, Y.; Hu, W.; Katipally, K.; Littke, A.; Pedro, A.; Qiu, Y.; Sandoval, M.; Schild, R.; Soltani, M.; Tedesco, A.; Vanyo, D.; Vemishetti, P.; Waltermire, R. E., The First Kilogram Synthesis of Beclabuvir, an HCV NS5B Polymerase Inhibitor. *Org. Process Res. Dev.* **2018,** *22* (10), 1393-1408.
21. Sullivan, R. J.; Freure, G. P. R.; Newman, S. G., Overcoming Scope Limitations in Cross-Coupling of Diazo Nucleophiles by Manipulating Catalyst Speciation and Using Flow Diazo Generation. *ACS Catal.* **2019,** *9* (6), 5623-5630.
22. Muller, S. T.; Murat, A.; Maillos, D.; Lesimple, P.; Hellier, P.; Wirth, T., Rapid Generation and Safe Use of Carbenes Enabled by a Novel Flow Protocol with In-line IR spectroscopy. *Chem. Eur. J.* **2015,** *21* (19), 7016-7020.
23. Deadman, B. J.; O'Mahony, R. M.; Lynch, D.; Crowley, D. C.; Collins, S. G.; Maguire, A. R., Taming tosyl azide: the development of a scalable continuous diazo transfer process. *Org. Biomol. Chem.* **2016,** *14* (13), 3423-3431.
24. Yu, Z.; Dong, H.; Xie, X.; Liu, J.; Su, W., Continuous-Flow Diazotization for Efficient Synthesis of Methyl 2-(Chlorosulfonyl)benzoate: An Example of Inhibiting Parallel Side Reactions. *Org. Process Res. Dev.* **2016,** *20*, 2116-2123.

25. Audubert, C.; Gamboa Marin, O. J.; Lebel, H., Batch and Continuous-Flow One-Pot Processes using Amine Diazotization to Produce Silylated Diazo Reagents. *Angew. Chem. Int. Ed.* **2017,** *56* (22), 6294-6297.
26. Pieber, B.; Kappe, C. O., Generation and Synthetic Application of Trifluoromethyl Diazomethane Utilizing Continuous Flow Technologies. *Org. Lett.* **2016,** *18* (5), 1076-1079.
27. Lehmann, H., A scalable and safe continuous flow procedure for in-line generation of diazomethane and its precursor MNU. *Green Chem.* **2017,** *19* (6), 1449-1453.
28. Levesque, E.; Laporte, S. T.; Charette, A. B., Continuous Flow Synthesis and Purification of Aryldiazomethanes through Hydrazone Fragmentation. *Angew. Chem.* **2017,** *129*, 855-859.
29. Maurya, R. A.; Park, C. P.; Lee, J. H.; Kim, D. P., Continuous in situ generation, separation, and reaction of diazomethane in a dual-channel microreactor. *Angew. Chem. Int. Ed.* **2011,** *50*, 5952-5955.
30. Mastronardi, F.; Gutmann, B.; Kappe, C. O., Continuous Flow Generation and Reactions of Anhydrous Diazomethane Using a Teflon AF-2400 Tube-in-Tube Reactor. *Org. Lett.* **2013,** *15* (21), 5590–5593.
31. Wernik, M.; Poechlauer, P.; Schmoelzer, C.; Dallinger, D.; Kappe, C. O., Design and Optimization of a Continuous Stirred Tank Reactor Cascade for Membrane-Based Diazomethane Production: Synthesis of α-Chloroketones. *Org. Proc. Res. & Dev.* **2019,** *23*, 1359-1368.
32. Sheeran, J. W.; Campbell, K.; Breen, C. P.; Hummel, G.; Huang, C.; Datta, A.; Boyer, S. H.; Hecker, S. J.; Bio, M. M.; Fang, Y.-Q.; Ford, D. D.; Russell, M. G., Scalable On-Demand Production of Purified Diazomethane Suitable for Sensitive Catalytic Reactions. *Org. Process Res. Dev.* **2021,** *25* (3), 522-528.
33. Poh, J. S.; Tran, D. N.; Battilocchio, C.; Hawkins, J. M.; Ley, S. V., A Versatile Room-Temperature Route to Di- and Trisubstituted Allenes Using Flow-Generated Diazo Compounds. *Angew. Chem. Int. Ed.* **2015,** *54* (27), 7920-7923.
34. Roda, N. M.; Tran, D. N.; Battilocchio, C.; Labes, R.; Ingham, R. J.; Hawkins, J. M.; Ley, S. V., Cyclopropanation using flow-generated diazo compounds. *Org. Biomol. Chem.* **2015,** *13* (9), 2550-2554.
35. Tran, D. N.; Battilocchio, C.; Lou, S. B.; Hawkins, J. M.; Ley, S. V., Flow chemistry as a discovery tool to access sp(2)-sp(3) cross-coupling reactions via diazo compounds. *Chem. Sci.* **2015,** *6* (2), 1120-1125.
36. Poh, J. S.; Makai, S.; von Keutz, T.; Tran, D. N.; Battilocchio, C.; Pasau, P.; Ley, S. V., Rapid Asymmetric Synthesis of Disubstituted Allenes by Coupling of Flow-Generated Diazo Compounds and Propargylated Amines. *Angew. Chem. Int. Ed.* **2017,** *56* (7), 1864-1868.
37. Nicolle, S. M.; Hayes, C. J.; Moody, C. J., Alkyl halide-free heteroatom alkylation and epoxidation facilitated by a recyclable polymer-supported oxidant for the in-flow preparation of diazo compounds. *Chem. Eur. J.* **2015,** *21* (12), 4576-4579.
38. Rackl, D.; Yoo, C. J.; Jones, C. W.; Davies, H. M. L., Synthesis of Donor/Acceptor-Substituted Diazo Compounds in Flow and Their Application in Enantioselective Dirhodium-Catalyzed Cyclopropanation and C-H Functionalization. *Org. Lett.* **2017,** *19* (12), 3055-3058.
39. Yoo, C. J.; Rackl, D.; Liu, W.; Hoyt, C. B.; Pimentel, B.; Lively, R. P.; Davies, H. M. L.; Jones, C. W., An Immobilized-Dirhodium Hollow-Fiber Flow Reactor for Scalable and Sustainable C-H Functionalization in Continuous Flow. *Angew. Chem. Int. Ed.* **2018,** *57*, 10923-10927.

40. Liu, W.; Twilton, J.; Wei, B.; Lee, M.; Hopkins, M. N.; Bacsa, J.; Stahl, S. S.; Davies, H. M. L., Copper-Catalyzed Oxidation of Hydrazones to Diazo Compounds Using Oxygen as the Terminal Oxidant. *ACS Catal.* **2021,** *11* (5), 2676-2683.
41. Wei, B.; Hatridge, T. A.; Jones, C. W.; Davies, H. M. L., Copper-catalyzed Oxidation of Hydrazones to Diazo Compounds in Continuous-Flow and Their Application in Dirhodium-Catalyzed Enantioselective Cyclopropanation Reactions. **2021**.
42. Badger, G. M.; Sasse, W. H. F., The Action of Metal Catalysts on Pyridines. In *Advances in Heterocyclic Chemistry Volume 2*, 1963; pp 179-202.
43. Davies, H. M.; Walji, A. M.; Nagashima, T., Simple Strategy for the Immobilization of Dirhodium Tetraprolinate Catalysts Using a Pyridine-Linked Solid Support. *J. Am. Chem. Soc.* **2004,** *126*, 4271-4280.
44. Davies, H. M.; Hansen, T.; Churchill, M. R., Catalytic Asymmetric C-H Activation of Alkanes and Tetrahydrofuran. *J. Am. Chem. Soc.* **2000,** *122*, 3063-3070.
45. Wei, B.; Sharland, J. C.; Lin, P.; Wilkerson-Hill, S. M.; Fullilove, F. A.; McKinnon, S.; Blackmond, D. G.; Davies, H. M. L., In Situ Kinetic Studies of Rh(II)-Catalyzed Asymmetric Cyclopropanation with Low Catalyst Loadings. *ACS Catal.* **2019,** *10*, 1161-1170.
46. Zhao, X.; Zhang, Y.; Wang, J., Recent developments in copper-catalyzed reactions of diazo compounds. *Chem. Commun.* **2012,** *48* (82), 10162-10173.
47. Gavriilidis, A.; Constantinou, A.; Hellgardt, K.; Hii, K. K.; Hutchings, G. J.; Brett, G. L.; Kuhn, S.; Marsden, S. P., Aerobic oxidations in flow: opportunities for the fine chemicals and pharmaceuticals industries. *React. Chem. Eng.* **2016,** *1* (6), 595-612.
48. Greene, J. F.; Hoover, J. M.; Mannel, D. S.; Root, T. W.; Stahl, S. S., Continuous-Flow Aerobic Oxidation of Primary Alcohols with a Copper(I)/TEMPO Catalyst. *Org. Process Res. Dev.* **2013,** *17* (10), 1247-1251.
49. Vanoye, L.; Aloui, A.; Pablos, M.; Philippe, R.; Percheron, A.; Favre-Reguillon, A.; Bellefon, C. d., A Safe and Efficient Flow Oxidation of Aldehydes with O2. *Org. Lett.* **2013,** *15* (23), 5978-5981.
50. He, Z.; Jamison, T. F., Continuous-flow synthesis of functionalized phenols by aerobic oxidation of Grignard reagents. *Angew. Chem. Int. Ed.* **2014,** *53* (13), 3353-3357.
51. Greene, J. F.; Preger, Y.; Stahl, S. S.; Root, T. W., PTFE-Membrane Flow Reactor for Aerobic Oxidation Reactions and Its Application to Alcohol Oxidation. *Org. Process Res. Dev.* **2015,** *19* (7), 858-864.
52. Al-Rifai, N.; Galvanin, F.; Morad, M.; Cao, E.; Cattaneo, S.; Sankar, M.; Dua, V.; Hutchings, G.; Gavriilidis, A., Hydrodynamic effects on three phase micro-packed bed reactor performance – Gold–palladium catalysed benzyl alcohol oxidation. *Chem. Eng. Sci.* **2016,** *149*, 129-142.
53. Pintar, A.; Bercic, G.; Levec, J., Catalytic liquid-phase oxidation of aqueous phenol solutions in a trickle-bed reactor. *Chem. Eng. Sci.* **1997,** *52*, 4143-4153.
54. Mata, A. R.; Smith, J. M., Oxidation of Sulfur Dioxide in a Trickle-bed Reactor. *Chem. Eng. J.* **1981,** *22*, 229-235.
55. Ranade, V. V.; Chaudhari, R. V.; Gunjal, P. R., Hydrodynamics and Flow Regimes. In *Trickle Bed Reactors*, Elsevier: 2011; pp 25-75.
56. Losey, M. W.; Schmidt, M. A.; Jensen, K. F., Microfabricated Multiphase Packed-Bed Reactors: Characterization of Mass Transfer and Reactions. *Ind. Eng. Chem. Res.* **2001,** *40* (12), 2555-2562.

57. Yue, J.; Chen, G.; Yuan, Q.; Luo, L.; Gonthier, Y., Hydrodynamics and mass transfer characteristics in gas–liquid flow through a rectangular microchannel. *Chem. Eng. Sci.* **2007,** *62* (7), 2096-2108.
58. Alsolami, B. H.; Berger, R. J.; Makkee, M.; Moulijn, J. A., Catalyst Performance Testing in Multiphase Systems: Implications of Using Small Catalyst Particles in Hydrodesulfurization. *Ind. Eng. Chem. Res.* **2013,** *52* (26), 9069-9085.
59. Guptill, D. M.; Davies, H. M., 2,2,2-Trichloroethyl aryldiazoacetates as robust reagents for the enantioselective C-H functionalization of methyl ethers. *J. Am. Chem. Soc.* **2014,** *136*, 17718-17721.
60. Likhar, P. R.; Roy, S.; Roy, M.; Kantam, M. L.; De, R. L., Silica immobilized copper complexes: Efficient and reusable catalysts for N-arylation of N(H)-heterocycles and benzyl amines with aryl halides and arylboronic acids. *J. Mol. Catal. A: Chem.* **2007,** *271*, 57-62.
61. Donia, A. M.; Atia, A. A.; El-Boraey, H.; Mabrouk, D. H., Uptake studies of copper(II) on glycidyl methacrylate chelating resin containing Fe2O3 particles. *Sep. Purif. Technol.* **2006,** *49*, 64-70.
62. Wu, X.; Gorden, A. E. V., 2-Quinoxalinol salen ligands incorporated into functionalized resins for selective solid-phase extraction of copper(II). *Tetrahedron Lett.* **2008,** *49* (35), 5200-5203.
63. Musaev, D. G.; Liebeskind, L. S., On the Mechanism of Pd(0)-Catalyzed, Cu(I) Carboxylate-Mediated Thioorganic-Boronic Acid Desulfitative Coupling. A Non-innocent Role for Carboxylate Ligand. *Organometallics* **2009,** *28*, 4639-4642.
64. Gruttadauria, M.; Giacalone, F.; Noto, R., "Release and catch" catalytic systems. *Green Chem.* **2013,** *15*, 2608-2618.
65. Weissman, S. A.; Anderson, N. G., Design of Experiments (DoE) and Process Optimization. A Review of Recent Publications. *Org. Process Res. Dev.* **2014,** *19* (11), 1605-1633.
66. Long, B.; Ryan, K. M.; Padrela, L., Investigating Process Variables and Additive Selection To Optimize Polymorphic Control of Carbamazepine in a CO2 Antisolvent Crystallization Process. *Org. Process Res. Dev.* **2020,** *24* (6), 1006-1017.
67. Dedè, F.; Piccolo, O.; Vigo, D., Dimethyl Fumarate: Heterogeneous Catalysis for the Development of an Innovative Flow Synthesis. *Org. Process Res. Dev.* **2021,** *25* (2), 292-299.
68. Lamberto, D. J.; Neuhaus, J., Robust Process Scale-Up Leveraging Design of Experiments to Map Active Pharmaceutical Ingredient Humid Drying Parameter Space. *Org. Process Res. Dev.* **2021,** *25* (2), 239-249.
69. Al-Dahhan, M. H.; Dudukovic, M. P., Catalyst Bed Dilution for Improving Catalyst Wetting in Laboratory Trickle-Bed Reactors. *AIChE J.* **1996,** *42* (9), 2594-2606.
70. Pereira, C. J.; Leib, T. M., Reactors. In *Perry's Chemical Engineers' Handbook*, 8 ed.; Green, D. W., Ed. The McGraw-Hill Companies, Inc.: 2008; pp 14-18.
71. Briones, J. F.; Davies, H. M. L., Rh2(S-PTAD)4-catalyzed asymmetric cyclopropenation of aryl alkynes. *Tetrahedron* **2011,** *67* (24), 4313-4317.
72. Davies, H. M. L.; Stafford, D. G.; Hansen, T., Catalytic Asymmetric Synthesis of Diarylacetates and 4,4-Diarylbutanoates. A Formal Asymmetric Synthesis of (+)-Sertraline. *Org. Lett.* **1999,** *1* (2), 233-236.
73. Wang, X.; Abrahams, Q. M.; Zavalij, P. Y.; Doyle, M. P., Highly regio- and stereoselective dirhodium vinylcarbene induced nitrone cycloaddition with subsequent cascade carbenoid aromatic cycloaddition/N-O cleavage and rearrangement. *Angew. Chem. Int. Ed.* **2012,** *51*, 5907-5910.

74. Vaitla, J.; Boni, Y. T.; Davies, H. M. L., Distal Allylic/Benzylic C-H Functionalization of Silyl Ethers Using Donor/Acceptor Rhodium(II) Carbenes. *Angew. Chem. Int. Ed.* **2020,** *59* (19), 7397-7402.
75. Sharland, J. C.; Wei, B.; Hardee, D. J.; Hodges, T. R.; Gong, W.; Voight, E. A.; Davies, H. M. L., Role of Additives to Overcome Limitations of Intermolecular Rhodium-Catalyzed Asymmetric Cyclopropanation. *ChemRxiv. Preprint.* **2021,** *https://doi.org/10.26434/chemrxiv.14479593.v1*.